The charge density of urea from synchrotron diffraction data

Henrik Birkedal,[a]*‡ **Dennis Madsen,**[b]*§ **Ragnvald H. Mathiesen,**[c]¶ **Kenneth Knudsen,**[d]‡‡ **Hans-Peter Weber,**[d,a] **Philip Pattison**[d,a] **and Dieter Schwarzenbach**[a]

[a]Laboratory of Crystallography, Swiss Federal Institute of Technology, BSP, CH-1015 Lausanne, Switzerland, [b]European Synchrotron Radiation Facility, Rue Jules Horowitz 6, BP 220, F-38043 Grenoble CEDEX, France, [c]Institutt for Fysikk, NTNU, N-7491 Trondheim, Norway, and [d]Swiss–Norwegian Beam Lines at ESRF, Rue Jules Horowitz 6, BP 220, F-38043 Grenoble CEDEX, France. Correspondence e-mail: hbirkedal@chem.au.dk, dnnm@novonordisk.com

The charge density of urea is studied using very high precision single-crystal synchrotron-radiation diffraction data collected at the Swiss–Norwegian Beam Lines at ESRF. An unprecedented resolution of 1.44 Å^{-1} in $\sin\theta/\lambda$ is obtained at 123 K. The optimization of the experiment for charge-density studies is discussed. The high precision of the data allowed the refinement of a multipole model extending to hexadecapoles and quadrupoles on the heavy and H atoms, respectively, as well as a liberal treatment of radial functions. The topological properties of the resulting electron density are analysed and compared with earlier experimental results as well as with periodic Hartree–Fock calculations. The properties of the strongly polarized C—O bond agree with trends derived from previous experimental results while the *ab initio* calculations differ significantly. The results indicate that the description of the C—O bond requires more flexible basis sets in the theoretical calculations. The calculated integrated atomic charges are much larger than the observed ones. It is suggested that the present experimental results provide new target values for validation of future *ab initio* calculations. The molecular dipole moment derived from the integrated atomic properties is the same as the one obtained from the multipole model even though the individual atomic contributions differ. Comparison with literature data for urea in solution and the gas phase yields a dipole enhancement in the solid of about 1.5 D. The thermal expansion of urea is determined using synchrotron powder diffraction data. With decreasing temperature, an increasing anisotropic strain is observed.

1. Introduction

Urea has attracted significant interest in the charge-density community because it is a simple, chemically interesting, non-centrosymmetric structure (Swaminathan, Craven, Spackman & Stewart, 1984; Spackman & Byrom, 1997; Zavodnik *et al.*, 1999; Spackman *et al.*, 1999; de Vries *et al.*, 2000). In particular, it has served as a model structure for studies of phase retrieval in non-centrosymmetric structures. Urea has been extensively studied with many techniques. Single-crystal neutron diffraction studies have been performed by Swaminathan, Craven &

McMullan (1984) and in several previous works cited therein. Swaminathan, Craven & McMullan (1984) collected full data sets at 12, 60 and 123 K with additional determination of lattice parameters at 30, 90, 150 and 173 K. Hereafter we refer to this study as SCM. Two earlier experimental charge-density studies have been published. Swaminathan, Craven, Spackman & Stewart (1984), hereafter SCSS, measured at 123 K the sector *hkl*, $h \geq k$, to a maximum of 1.15 Å^{-1} in $\sin\theta/\lambda$. Zavodnik *et al.* (1999), hereafter ZSTVF, measured a more complete data set to the same resolution but at 148 K. They then used scaled values of the neutron H-atom parameters of SCM in the X-ray refinements. They obtained displacement parameters of the heavy atoms from a high-order refinement and used only the 145 reflections at $\sin\theta/\lambda \leq 0.7$ Å^{-1} for the multipole refinement.

Urea was the first molecular crystal to be studied with fully periodic Hartree–Fock calculations by Dovesi *et al.* (1990) using the *CRYSTAL* program. This study was followed by the

---

‡ Present address: Department of Chemistry, University of Aarhus, Langelandsgade 140, DK-8000 Aarhus, Denmark.
§ Present address: Novo Nordisk A/S, Department of Scientific Computing, Novo Nordisk Park, A2P, DK-2760 Måløv, Denmark
¶ Present address: SINTEF, Applied Physics Department, N-7465 Trondheim, Norway.
‡‡ Present address: Institute for Energy Technology, Physics Department, N-2007 Kjeller, Norway.

first application of the quantum theory of atoms in molecules (AIM) on a molecular crystal by Gatti *et al.* (1994), using *CRYSTAL* in combination with Gatti's AIM program *TOPOND*. The first study used the 6-21G(d,p) basis set while the latter one employed 6-31G(d,p). It should be mentioned that such relatively small basis sets perform better in periodic than in molecular calculations (Pisani *et al.*, 1988; Pisani, 1996). The AIM results were extended by Gatti & Cargnoni (1997). Gatti (1999) has kindly provided us with his AIM results of periodic RHF calculations using the geometry from the 123 K SCM study and three different basis sets: 6-21G(d,p), 6-31G(d,p) and 6-311G(d,p). The discussions of the present work refer to these new calculations (Gatti, 1999), which are slightly different from the published ones (Gatti *et al.*, 1994; Gatti & Cargnoni, 1997).

The crystal structure of urea shows several chemically remarkable features. Fig. 1 shows the molecular structure and labelling scheme. The molecule adopts a flat conformation in the crystal with site symmetry $mm2$. In contrast, the isolated molecule is non-planar, the NH_2 groups being twisted slightly out of the molecular plane as determined by microwave spectroscopy (Godfrey *et al.*, 1997) and by *ab initio* calculations (Dixon & Matsuzawa, 1994; Ha & Puebla, 1994; Rasul *et al.*, 1994; Godfrey *et al.*, 1997; Rousseau *et al.*, 1998; Miao *et al.*, 2000). It is now accepted that the C_2 molecular structure is the most stable followed by a C_s conformation. The C_{2v} structure found in the crystal is a saddle point separating these two stable conformers. Another most interesting aspect of the crystal structure of urea is the hydrogen-bond pattern where the O atom accepts four hydrogen bonds, see Fig. 1. This is extremely rare. The only other such structures we are aware of are found in the intriguing series of host–guest molecular complexes based on a host derived from calix[4]pyrrole (Bonomo *et al.*, 1999; Anzenbacher *et al.*, 1999).[1]
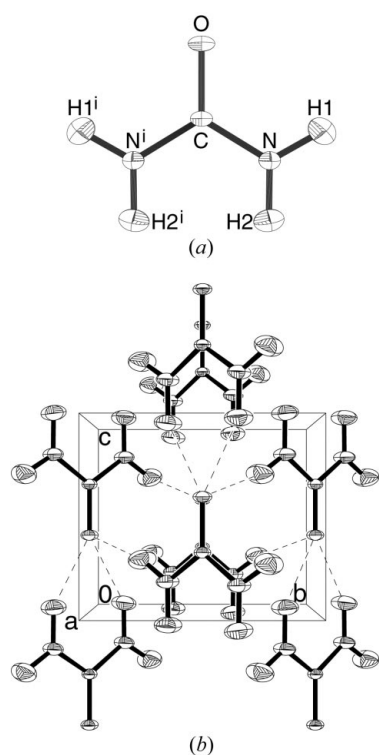
Urea is known to undergo several phase transitions at moderate pressures (<0.4 GPa at room temperature). The structure of the first high-pressure phase has been solved (Bonin *et al.*, 1999) but the coordinates are not available at the present time. However, it is clear that the columnar structure (Fig. 1b) collapses. The molecule becomes non-planar as in the gas phase and the O atom accepts only three hydrogen bonds. Thus, small pressure is sufficient to distort the open columnar structure at the expense of a reduction of the number of hydrogen bonds per O atom.

Here we report a high-precision study of the charge density of urea using synchrotron diffraction data collected at the Swiss–Norwegian Beam Lines (SNBL) at the European Synchrotron Radiation Facility (ESRF), Grenoble, France. The use of synchrotron radiation led to a data set of unprecedented resolution and precision, which in turn allowed the use of a very extensive multipole model. The charge density thus obtained can be used as a benchmark for testing theory that, as will become apparent, is still lagging behind experiment in this case.

2. Experimental

All diffraction measurements were performed at the bending magnet based Swiss–Norwegian Beam Lines (SNBL) at ESRF.

2.1. Powder diffraction – thermal expansion and anisotropic strain

The sample was mounted in a 0.7 mm borosilicate capillary. High-resolution powder data were collected at the SNBL B-station. The wavelength, $\lambda = 0.64791$ Å, was calibrated with an Si standard. Data were collected at four temperatures: 295, 120, 80 and 10 K. For the three low-temperature collections, the temperature was controlled by a modified STVP-400 open-flow helium cryostat from Janis Research Company. The step size, $\Delta 2\theta$, was $0.005°$ in all measurements. For 295, 120 and 80 K, the counting time was 1 s step^{-1} while, for 10 K, it was 4 s step^{-1} for $2\theta = 9$–$19°$ and 8 s step^{-1} elsewhere. The data sets cover 8.5–21.995°, except for the 10 K data set which starts at 9.0°. The powder patterns displayed significant anisotropic peak broadening. LeBail fits (LeBail *et al.*, 1988) were performed with *GSAS* (Larson & Von Dreele, 1994) using the Stephens (1999) anisotropic broadening model in combination with the Thompson *et al.* (1987) parameterization of the pseudo-Voigt function and the Finger *et al.* (1994) peak

Figure 1
(*a*) Molecular structure of urea and labelling scheme; (*b*) perspective view of the crystal structure along the *a* axis. The 50% probability ellipsoids represent the harmonic ADPs at 123 K. Symmetry operation (i) is $x, 1 - y, z$.

---

[1] Ammonium cyanate was originally thought to provide another example of fourfold acceptor O atoms, based on an X-ray powder structure (Dunitz *et al.*, 1998). However, it was recently shown by neutron powder diffraction that the hydrogen-bond acceptor is actually not the cyanate O atom but rather the cyanate N atom, which acts as a fourfold acceptor (MacLean *et al.*, 2003).

asymmetry correction. The fits with observations and a table containing the profile parameters are given in the supplementary material (Fig. S1, Table S1), which also contains a more detailed discussion of the anisotropic broadening.[2]

The resulting lattice parameters are shown in Fig. 2. They increase smoothly with increasing temperature. The neutron measurements are slightly off the curves, are somewhat larger and show a much larger scatter. The thermal expansion is evidently strongly anisotropic (Swaminathan, Craven & McMullan, 1984). It was modelled by a single effective Einstein oscillator, $\ln(V/V_0) = (k_B n/BV_m)\{\gamma\Theta/[\exp(\Theta/T) - 1]\}$, where V_0 is the cell volume at zero temperature, k_B the Boltzmann constant, n the number of atoms per unit cell, B the bulk modulus, V_m the molar volume, γ a Grüneisen parameter and Θ the effective Einstein temperature (Wang & Reeber, 2000). Since we have not measured B, the constants were combined into an effective pre-factor $A_E = \gamma k_B n/BV_m$. The fits have correlation coefficients larger than 0.9996, the final fitting parameters are $V_0(a) = 5.5640\,(11)$ Å, $\Theta(a) = 280\,(31)$ K, $A_E(a) = 9.4\,(5)$, $V_0(c) = 4.68316\,(6)$ Å, $\Theta(c) = 268\,(6)$ K and $A_E(c) = 2.19\,(2)$. Interestingly, the Einstein temperatures of a and c are essentially equal so that the anisotropy of the thermal expansion stems from the pre-factor, which includes the Grüneisen parameter and the compressibility. The difference in stiffness along the two directions appears to be responsible for the difference in thermal expansion.

The powder diffraction patterns display anisotropic micro-strain broadening and the peak widths increase with decreasing temperature.[2] Tentatively, we suggest that this is linked to a phase transition. No anomalies have been detected in the heat capacity at ambient pressure (Ruehrwein & Huffman, 1946; Andersson et al., 1993) but the transition pressure of the first pressure-induced phase transition is reduced at lower temperatures (Andersson & Ross, 1994) and it has been predicted that the high-pressure phase might become thermodynamically stable at low temperatures. The powder diagrams display neither peak splitting nor the appearance of new peaks. However, Andersson & Ross (1994) found that the phase transition could be induced only under isothermal pressurization and not under isobaric cooling. Hence a suppressed phase transition may be the reason for the anisotropic strain broadening. Whether this phase transition is suppressed by thermodynamics or by kinetics is unclear.

2.2. Single-crystal measurements

2.2.1. Beamline layout and diffractometer. A significant effort was invested in the optimization of the data-collection parameters. Station A of SNBL is equipped with a six-circle κ diffractometer from KUMA diffraction (KM6-CH) specifi-

cally constructed for off-vertical plane diffractometry and this use of the diffractometer has been discussed previously (Thorkildsen et al., 1999, 2000). Here, we used the diffractometer as a standard four-circle κ instrument with the detector circle (2θ) in the vertical plane to profit from the linear polarization of the radiation.

Station A of SNBL offers two types of optics: parallel-beam and focusing optics. In the parallel-beam configuration, the monochromator contains two flat Si(111) crystals arranged in a fixed-exit geometry. In the focusing set-up, the optics consists of a vertically collimating Rh-coated Si mirror, a fixed-exit Si(111) monochromator where the second crystal is sagitally bent for horizontal focusing, followed by an Rh-coated Si mirror that provides vertical focusing. We collected test data using both optical configurations. The best results, in terms of internal consistency of the data sets, were obtained with parallel-beam optics. We attribute this to somewhat more stable beam conditions for this mode. For charge-density studies, where the crystals are of 'normal' size, the intensity gained by focusing is not needed. Indeed, the main advantages of synchrotron radiation are the low inherent background (stemming from the low divergence) and the high degree of monochromaticity, which make weak reflections much easier to measure. Therefore, parallel-beam optics was chosen for the final data collection.

2.2.2. Charge-density data collection. An overview of the single-crystal data-collection parameters is given in Table 1, which compares our measurements with those of SCSS and ZSTVF. The wavelength was determined from the room-temperature lattice parameter of a CaF_2 reference crystal refined from the setting angles of 24 reflections. The data-collection temperature, controlled with an Oxford cryosystem N_2 cooling system, was 123 K to allow use of the SCM neutron H-atom parameters in the charge-density refinements. The cell parameters were determined from the angles of 17 centred reflections. The results are within one s.u. of the values obtained from the powder diffraction data (Fig. 2). This very
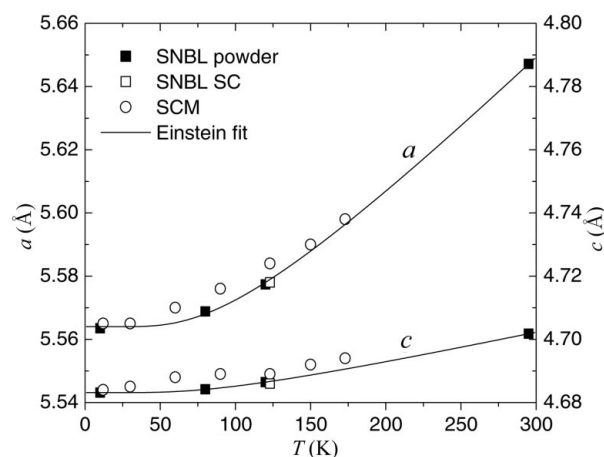
Figure 2
Temperature dependence of the lattice parameters of urea. The solid lines are fits to the lattice parameters from powder diffraction. Also shown are the SCM (Swaminathan, Craven & McMullan, 1984) neutron and the single-crystal (SC) parameters of the present work.

---

[2] Supplementary material, including a CIF file and structure factors, figures showing the quality of the Le Bail fits, tabulations of results of the Le Bail fits, a discussion of the anisotropic peak broadening, tables and discussion of topological properties of the electron density, and an overview of previous experimental determinations of the dipole moment of urea in solution and gas phase are available from the IUCr electronic archives (Reference: XC5013). Services for accessing these data are described at the back of the journal.

research papers

Table 1
Data collections on urea.

SCSS is Swaminathan, Craven, Spackman & Stewart (1984), ZSTVF is Zavodnik *et al.* (1999). The two values under ZSTVF in the refinement part of the table refer to the full and low-angle data set, respectively, see text. $R_\sigma = \sum \sigma(F_o^2)/\sum F_o^2$, calculated from the deposited data of SCSS and ZSTVF. R_{int} for SCSS refers only to averaging of reference reflections.

	Present	SCSS	ZSTVF
Experimental			
T (K)	123 (2)	123 (2)	148 (1)
a (Å)	5.5780 (6)	5.578 (1)	5.5890 (5)
c (Å)	4.6860 (7)	4.686 (1)	4.6947 (4)
λ (Å)	0.5996 (1)	0.7107	0.7069
μ (mm^{-1})	0.07	0.11	0.127
Crystal size (mm)	0.09×0.13×0.23	0.40×0.40×0.25	0.30×0.30×0.35
Absorption correction	None	None	Numerical
Scan type	ω	ω–2θ	ω–2θ
No. of reflections			
measured	3942	'A sector'	1971
unique	1045	318	412/145
R_{int}	0.0141	0.03	0.015
R_σ	0.0153	0.0242	0.0045
$\langle F_o^2/\sigma(F_o^2)\rangle$	49.9	29.3	148.5
$\sin\theta/\lambda_{max}$ (Å^{-1})	1.44	1.15	1.15
TDS correction	None	None	Peak tail fits
Refinement			
Refinement on	F^2	F	F
No. of parameters	77	34	28/29
$wR(F)$	0.0054	0.015	0.028/0.011
$R(F)$	0.0204	0.035	0.025/0.008
$wR(F^2)$	0.0108		
$R(F^2)$	0.0071		
S	1.1661	1.57	1.64/1.09

good agreement indicates that the temperature of the single-crystal experiment was estimated correctly.

The data collection took about three days and covered a hemisphere of reciprocal space, selected so as to minimize vibrations induced by the cold stream. Initial test measurements showed marked improvement when the sample mount was kept roughly parallel to the gas stream. The crystals had a tendency to crack when the temperature was lowered. Neither of the previous works mention this problem. It is possible that the cracking only becomes visible at the increased resolution of the synchrotron. Cooling was most successful with a sample that had a somewhat broad room-temperature mosaic spread because a slightly strained crystal probably gives better data than a cracked one. Reflection intensities were measured with ω scans that, owing to the negligible dispersion of the synchrotron beam, can be expected to give the best peak sampling (Blessing, 1987). The scan width was kept constant at $\Delta\omega = 1.0°$. A small set of strong low-angle reflections was measured with a scan width of $1.2°$ to verify that scan-truncation errors did not occur. The reflections were scanned continuously using 100 bins per reflection. This is faster than and at least as reliable as a step scan with 100 steps. The strongest reflections were measured with Cu foil attenuators. For most of them, the standard pre-detector attenuator was sufficient, but for the very strongest reflections additional attenuators were placed in the incident beam. Attenuator absorptions were derived from measurements with and without filter.

The data set extends to 1.44 Å^{-1} (Table 1), while the sample scattered to higher angles. However, at the highest angles, $2\theta \simeq 120°$, the detector arm was at risk of colliding with other equipment in the experimental hutch.

2.2.3. Data reduction. Data reduction was performed using the *XD_RED* program of Mathiesen (2001), updated to accommodate synchrotron data from the KM6-CH diffractometer. It performs detailed error propagation calculations with inclusion of, in particular, the s.u.'s of the degree of polarization and the wavelength. The background was estimated from the first 9 and the last 9 steps of each scan. The degree of polarization of the polychromatic synchrotron beam was set to 0.95 (1). This value has been measured in earlier experiments at SNBL under slightly different conditions (Birkedal, 2000). *XD_RED* takes the effect of the monochromator explicitly into account and obtained a degree of polarization at the sample position of 0.952. The variance of a reflection includes an instrumental instability factor of $s = 0.002$, according to $\sigma^2(F_\mathbf{H}^2) = \sigma^2[I_\mathbf{H}(\text{net}) + [sI_\mathbf{H}(\text{net})]^2$, where $I_\mathbf{H}$ is the intensity.

2.2.4. Thermal diffuse scattering. Thermal diffuse scattering (TDS) may be large at high diffraction angles and at temperatures significantly above the Debye temperature, Θ_D. Θ_D of urea has been derived from heat-capacity measurements (Andersson *et al.*, 1993), using several different methods. The smallest value obtained was $\Theta_D = 135.0$ K. The present experiment, as well as that of SCSS, was performed at 123 K, below the Debye temperature. It was thus deemed safe to neglect the TDS correction, considering also that the temperature dependence of the elastic constants is unknown. ZSTVF corrected for TDS at 148 K by making linear fits to the tails of the diffraction peaks. In view of the anisotropic peak broadening, this procedure may lead to questionable results for our crystal.

2.2.5. Charge-density refinement. The *VALRAY* program system (Stewart *et al.*, 1998) was used for the full-matrix least-squares (LSQ) refinement based on F^2 and using experimental weights, $w(\mathbf{H}) = 1/\sigma^2[F_o^2(\mathbf{H})]$. All reflections were included in the refinement. The Hamilton (1965) R-factor-ratio test was used to verify that newly introduced parameters led to significant improvement in residuals.

The initial fractional coordinates and ADPs of N, C and O atoms were taken from SCSS. H-atom nuclear parameters were taken from the 123 K SCM neutron study and kept fixed during the refinement. Anharmonicity was included *via* refinement of third-order Gram–Charlier coefficients on N and O atoms, which led to significant improvement in residuals. Tests employing third-order parameters on C atoms as well did not lead to lower residuals. The multipole expansion was extended up to the hexadecapole level for C, N and O atoms and to the quadrupole level for H atoms. At all levels, population parameters above 3 s.u. were found

The radial functions of mono-, di- and quadrupoles for C, N and O atoms were the density-localized (van der Wal & Stewart, 1984) orbital products of Clementi & Roetti (1974). Let (is) designate an inner shell density localized orbital product and (os) an outer shell product. The following

Table 2
Parameters varied in the charge-density refinement.

The neutron results used for H atoms are from SCM. Radial functions are: † density localized orbital products, * κ refined; ‡ exponential, α refined (SCSS obtained α from multipole fits to isolated molecule RHF/6-31G(d,p) structure factors); exponential, κ refined. IAM = independent atom model.

	Present	SCSS	ZSTVF
Position	C, N, O	Neutron	High-angle IAM
U^{ij}	C, N, O	Neutron	High-angle IAM
C^{ijk}	N, O		
H atoms	Neutron	Neutron	Scaled neutron
Poles:			
mono	C†, N†, O†, H‡	C‡, N‡, O‡, H‡	C*, N*, O*, H*
di	C†, N†, O†, H‡	C‡, N‡, O‡, H‡	C*, N*, O*, H*
quadru	C†, N†, O†, H‡	C‡, N‡, O‡, H‡	C*, N*, O*
octu	C‡, N‡, O‡	C‡, N‡, O‡	C*, N*, O*
hexadeca	C‡, N‡, O‡		C*
Extinction	Becker & Coppens (1974)	None	Zachariasen (1967)

products were used: core monopoles (is)(is), valence monopoles (os)(os), valence dipoles $(2p)$(os), and valence quadrupoles $(2p)(2p)$. For the valence mono-, di- and quadrupoles, a common κ parameter was refined for each atom. The radial functions of the higher poles (octu- and hexadecapoles) on C, N and O atoms and all radial functions on H atoms were described by exponential functions, $R_l(r) = [\alpha^{n_l+3}/(n_l + 2)!]r^{n_l} \exp(-\alpha_l r)$, with $n_l \geq l$ (Stewart, 1977). The initial values of α were standard molecular values (Hehre *et al.*, 1969, 1970) and n_l was set equal to l. In the final model, the α's were refined. The α parameters of the octu- and hexadecapoles were constrained to be equal for each atom type while all α's of the two H atoms were constrained to be equal. The core monopole populations were constrained to be equal, $P_c(C) = P_c(O) = P_c(N)$.

In Table 2, the present refinement is compared with the refinements of SCSS and ZSTVF. Our final model comprised 77 parameters. In addition to the nuclear and electron parameters shown in the table, an isotropic extinction parameter, g, with Lorentzian distribution of mosaic blocks (Becker &

Coppens, 1974) was refined. The final value $g = 0.016 (3) \times 10^{-4}$ rad^2 yields a lowest F_o^2/F_c^2 ratio of 0.974 for the 110 reflection – well within the regime where the description of extinction is adequate. The scale factor was not refined but estimated from the ratio between $F(000)$ and the sum of valence and core populations (Stewart, 1976). Its final value is 0.952 (6). The largest correlation coefficient was 0.95 between α_C and $P_{30}(C)$.

2.3. Analysis of the electron density: atoms in molecules

The electron density was analysed in terms of the theory of atoms in molecules (Bader, 1994). Integrated properties were obtained using the method of Flensburg & Madsen (2000). A similar algorithm has been used by Gatti (1999). For the integration of the experimental density, 5024 points were used to span the surface of C and N atoms while 2788 points were determined on the zero-flux surface of O atoms. For H atoms, 664 points were employed for each zero-flux surface. This gave an integration sampling between 10^5 and 10^6 points in each atomic basin.

3. Discussion of the single-crystal study

The internal agreement of our data set is comparable to the two previous studies, SCSS and ZSTVF, even though both the resolution and the number of averaged reflections are much larger. In Table 1, we compare the three data sets,[3] and in particular the values of R_σ and $\langle F_o^2/\sigma(F_o^2)\rangle$ whose significance depends of course on a proper estimation of the s.u.'s. The present values are significantly superior to those of SCSS as should be expected from the combination of repeated measurements and the benefits of synchrotron radiation. The values given by ZSTVF are even more impressive. For the fraction of our data set with the resolution of ZSTVF, we obtain $R_\sigma = 0.0067$ and $\langle F_o^2/\sigma(F_o^2)\rangle = 80.5$. A more detailed analysis of $\langle F_o^2/\sigma(F_o^2)\rangle$ for different groups of reflections and the rather large value of the goodness of fit S of ZSTVF suggests that ZSTVF may have underestimated the s.u.'s. In addition, the ZSTVF data set was corrected for TDS by fitting peak tails, but the anisotropic strain broadening observed in our powder measurements suggests other contributions to the tails.

Our refinement led to very small R values (Table 1) demonstrating the extremely good agreement between measurements and model. The residual density is shown in Fig. 3, which displays two maps; one map has been calculated with all reflections and the other one with the resolution $\sin\theta/\lambda_{max} = 1.15$ Å^{-1} of the two previous studies. The latter is completely flat while the former shows features amounting to ± 0.20 e Å^{-3}. This is due to the expected increase of the relative uncertainty $\sigma(F_o^2)/F_o^2$ at higher angles. It can thus be concluded that the refinement successfully reproduces the measured intensities.

Figure 3
Residual charge density in urea after multipole refinement, view on the molecular plane. Positive contours full lines, negative contours dashed, zero contour long dashes, intervals 0.05 e Å^{-3}. Map on the left calculated with all reflections, maximum and minimum contours ± 0.20 e Å^{-3}. Map on the right calculated with the resolution of SCSS and ZSTVF, $\sin\theta/\lambda_{max} = 1.15$ Å^{-1}.

---

[3] For these comparisons, the data sets of SCSS and ZSTVF were transformed from F to F^2. The s.u.'s were transformed according to $\sigma(F^2) = 2F\sigma(F)$.

Table 3
Nuclear parameters of urea.

First line: present study; second line: 123 K neutron results of SCM. H-atom parameters are not included as they were taken from the neutron refinement. The fractional coordinates are multiplied by 10^4, U^{ij} in units of 10^{-4} Å^2, C^{ijk} multiplied by 10^5. C and O atoms are on positions $(0, 1/2, z)$, site symmetry $2.mm$, the N atom is on position $(x, x+1/2, z)$, site symmetry $..m$.

	x	z	U^{11}	U^{33}	U^{12}	U^{13}
C		3282.1 (3)	151.9 (4)	67.5 (4)	−3.5 (6)	
		3280 (2)	147 (5)	65 (3)	1 (4)	
O		5963.4 (10)	195.8 (4)	66.5 (3)	16.4 (8)	
		5962 (2)	197 (6)	63 (4)	17 (5)	
N	1446.8 (7)	1790.1 (10)	293.1 (6)	95.6 (4)	−157.0 (7)	0.2 (3)
	1447 (1)	1785 (1)	286 (4)	95 (2)	−147 (2)	2 (3)

	C^{111}	C^{112}	C^{113}	C^{123}	C^{133}	C^{333}
O			−3.2 (9)	2 (4)		1.3 (5)
N	−6.5 (7)	5.8 (8)	18.8 (13)	−36 (3)	1.2 (7)	1.8 (6)

3.1. Geometry and thermal motion

Fractional coordinates and displacement parameters are given in Table 3. The agreement between the nuclear parameters obtained in the present study and the neutron results of SCM is excellent. All quantities are equal within two neutron s.u.'s except for z and U^{12} of the N atom where the difference is 5.1 and 5.0 neutron s.u.'s, respectively. This difference is due to the inclusion of anharmonicity in the present model, with particularly significant results for the N atom.

The SCM neutron displacement parameters were analysed by Capelli *et al.* (2000). They adjusted by LSQ a molecular mean-field model of rigid-body and low-frequency internal motion to the temperature dependence of the ADPs (Bürgi & Förtsch, 1999; Bürgi & Capelli, 2000; Bürgi *et al.*, 2000). They found that the pyramidalization of the N atom, which is partly responsible for the non-planarity of the molecule in the gas phase, is also important in the solid state. The largest anharmonic effect in the present model is in the out-of-plane N-atom motion, consistent with the analysis of Bürgi *et al.* (2000). The molecular geometry and the geometry of the hydrogen bonds[4] are given in Table S4 (supplementary material). The geometry agrees with the neutron data but the present results are significantly more precise. The molecular geometry in the gas phase (Godfrey *et al.*, 1997) presents some interesting differences from the solid state. The C=O bond is 0.036 Å shorter in the gas phase while the C−N bond is 0.040 Å longer. This difference is larger than what can be expected from the non-planarity only and has been explained as a direct effect of the extensive hydrogen bonding in the crystal (Keuleers *et al.*, 1999).

---

[4] All geometrical quantities involving H-atom positions and/or the positions of critical points have been calculated from the parameters after refinement. For quantities involving H atoms, the s.u.'s given by SCM were used. This is necessary as neither H-atom nor critical-point coordinates are variables in the least-squares-refinement process. The procedure neglects correlation between the parameters.

Table 4
Radial scaling parameters (Å^{-1}) for urea.

HSP are the standard molecular values used as starting point in the refinement (Hehre *et al.*, 1969, 1970).

	Present		SCSS	ZSTVF	HSP
	κ	α	α	κ	α
C	0.991 (4)	5.09 (10)	4.42 (8)	0.97 (1)	6.50
O	0.9784 (16)	9.1 (6)	9.6 (3)	0.98 (1)	8.50
N	1.002 (3)	7.2 (2)	7.97 (19)	0.98 (1)	7.37
H		4.38 (5)	4.91 (17)	1.02 (2)	4.69

3.2. Deformation density model

The refined multipole population parameters are presented in Table S3 (supplementary material). The present model extends further than the two previous ones since hexadecapoles are used on all heavy atoms, see Table 2. ZSTVF used hexadecapoles on C atoms only with the largest population parameter being only 3 s.u. In contrast, our hexadecapole parameters attain values of up to 6 s.u.'s. The current radial description is more flexible than either of the previous studies (Table 2). The exponents of the single exponentials used by SCSS, one α for each atom type, were not experimentally derived but calculated from a LSQ fit of an electron-density model to theoretical structure factors obtained by a 6-31G(d,p) RHF molecular calculation assuming a crystal consisting of non-interacting molecules. ZSTVF performed κ refinements but do not specify the radial functions used.

The refined radial parameters are given in Table 4, where we compare them with the SCSS, ZSTVF and the standard molecular exponents of Hehre *et al.* (1969, 1970), hereafter referred to as HSP. Fig. 4 shows the radial function for the C-atom octupole. The lower-order poles ($l \leq 2$), treated by κ refinement, were only slightly modified in the refinement. C and O atoms are expanded ($\kappa < 1$), but C atoms only slightly so. The inner poles on the N atom are unchanged within less than one s.u. For the higher poles, the O atom is contracted with respect to the HSP standard values while C, N and H atoms are more diffuse. In comparison with SCSS, where the values were refined with a scaling parameter common for all poles, the C atom is less diffuse while the other atoms are more
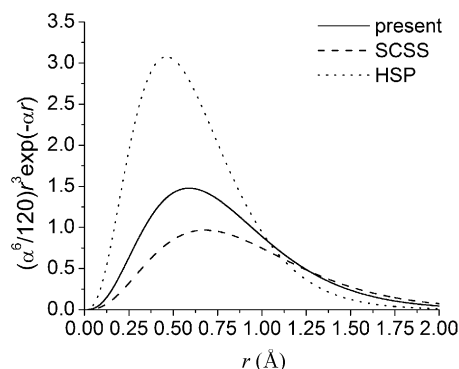
Figure 4
Normalized C-atom octupole radial function of urea.

diffuse. The C atom shows the largest variations. The maximum of the radial function (Fig. 4) is $r_{max} = n_l\alpha^{-1}$, which gives 0.46, 0.59 and 0.68 Å for the HSP standard exponent, the present refined one and the SCSS value, respectively. It is clear that the C atom in urea has more diffuse components than the standard HSP atom.

The need for flexible radial functions has been noted by Figgis *et al.* (1993) in their 9 K X–N study of $(ND_4)_2$-$(Cu(SO_4))_2 \cdot 6D_2O$. They conclude 'The molecular density is not described by simple κ modification of atomic radial functions'. They solved the problem by adding extra diffuse radial functions on some atoms but did not refine exponents. Volkov *et al.* (2000) investigated the difference between experimental and theoretical crystal charge densities by applying a multipole model to calculated structure factors. Theoretical structure factors at the periodic RHF/6-21G(d,p) and RHF/6-31G(d,p) level were calculated to a resolution of $\sin\theta/\lambda < 1.05$ Å^{-1}. The ensuing multipole refinements were subjected to local symmetry and chemical constraints and extended to octupoles only for the non-H atoms and to the quadrupole level for H atoms. Their principal conclusion was 'The main origin of the observed discrepancies is attributed to the nature of the radial functions in the experimental multipole model'. While their multipole modelling approach can be considered somewhat restricted, this conclusion shows that it is necessary to allow full flexibility in the radial functions.

3.3. Critical points

In Tables 5, S5, S6, S7 and S8, we present the critical points (CPs) of the electron density and compare them with the theoretical and ZSTVF results. The topology fulfils the Morse equation, $n(3,-3) - n(3,-1) + n(3,+1) - n(3,+3) = 0$ for periodic systems, and is thus consistent. A qualitative discussion of the topology is given in the supplementary material.
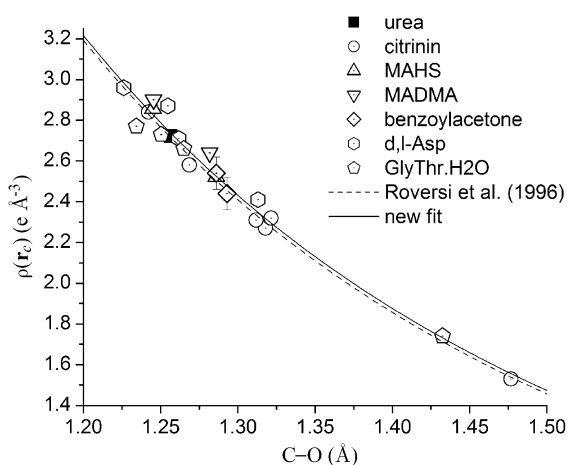
Figure 5
Relation between bond length D and $\rho(\mathbf{r}_c)$ for C—O bonds. Systems are citrinin (Roversi *et al.*, 1996), MAHS (methylammonium hydrogen succinate, Flensburg *et al.*, 1995), MADMA (methylammonium hydrogen maleate, Madsen *et al.*, 1998a), benzoylacetone (Madsen *et al.*, 1998b), D,L-Asp (Flaig *et al.*, 1998), Gly-L-Thr dihydrate (Dittrich *et al.*, 2000) and urea from the present study. Two exponential fits are given, one to the citrinin data 'Roversi *et al.* (1996)' and one to all the data 'new fit'.

The hydrogen-bonded columns create empty tunnels along the c axis (Swaminathan, Craven & McMullan, 1984). In these, the atomic surfaces of the N atoms meet, and the N atoms are thus bonded (in the topological sense) across the tunnel. The topology derived from the theoretical calculations (Gatti, 1999) shows exactly the same set of bond CPs (BCP).

The only qualitative difference between the *ab initio* and experimental electron densities is in the regions where the electron density is close to zero. In the experimental density, there is a minimum (C5) with negative $\rho(\mathbf{r}_c) = -0.0008$ (2) e Å^{-3}, *i.e.* practically zero. In addition, there is a minimum with a positive density (C4) with $\rho(\mathbf{r}_c) = 0.0030$ (1) e Å^{-3}. The first is situated in the 'walls' of the empty column mentioned above while the latter is situated close to the centre. Two ring critical points are also present (R5 and R6, Table S6) to fulfil the Morse equation. In the theoretical density, R5 and R6 are substituted by a single point R5' (see Table S7 for characteristics of the ring and cage critical points of the periodic *ab initio* calculations). The positivity of experimental electron densities is not guaranteed by the multipole model, while the *ab initio* calculations do not suffer from this problem. The local deficiency of the experimental model is not expected to have major consequences outside low-density regions.

Roversi *et al.* (1996) found that the value of the charge density in the BCP of C—O bonds in citrinin follows the relation $\rho(\mathbf{r}_c) = 6.063D^{-3.521}$, where the bond length D is in Å and $\rho(\mathbf{r}_c)$ in e Å^{-3}. We included several other values from the literature to get an idea of the quality of the relation, Fig. 5. The agreement is generally very good and the present value for urea is in extremely good agreement with the literature values. By fitting the curve to all the values, a new relation is obtained which is labelled 'new fit' in Fig. 5:[5] $\rho(\mathbf{r}_c) = 6.087(180)R^{-3.498(120)}$. Our value of $\rho(\mathbf{r}_c)$(C—O) is larger by 0.186 e Å^{-3} than that of ZSTVF. The agreement of our value with the host of other experimental values (Fig. 5) suggests that the result of ZSTVF is less accurate. The present value of the C—O Laplacian is about the same as has been found in the studies presented in Fig. 5. It is also close to the average values derived from nine amino acids by Flaig *et al.* (1999), who found −33.0 (40) and −34.9 (26) e Å^{-5} for the long and short carboxylate bond, respectively. The value of ZSTVF, −18.86 e Å^{-5}, seems to be too small.

The bond length and $\rho(\mathbf{r}_c)$ places the C—O bond between a typical double and single bond. The value of the ellipticity indicates a predominantly σ-type bond. The C—N bond is rather short, and shows relatively large values of $\rho(\mathbf{r}_c)$ and of ellipticity. This indicates a π contribution to the bond with charge delocalization over the O⋯C⋯N framework. The intermolecular interactions are all of closed-shell nature (Table S5), in agreement with the expectation for normal predominantly electrostatic hydrogen bonds.

---

[5] No s.u.'s on $\rho(\mathbf{r}c)$ are given by Flaig *et al.* (1998) for D,L-Asp. For the LSQ fit, the four observations from this study were, arbitrarily, assigned s.u.'s of 0.04 in order to permit using weighted LSQ.

Table 5
Intramolecular bond critical points in crystalline urea.

D is the bond length $A-B$, $D1$ is the distance from A to the BCP while $D2$ is the B–BCP distance. First line: present study; second: periodic RHF 6-21G(d,p); third: periodic RHF 6-31G(d,p); fourth: periodic RHF 6-311G(d,p); fifth: experimental density of ZSTVF.

	D (Å)	$D1$ (Å)	$D2$ (Å)	$\rho(\mathbf{r}_c)$ (e Å^{-3})	$\nabla^2\rho(\mathbf{r}_c)$ (e Å^{-5})	λ_1 (e Å^{-5})	λ_2 (e Å^{-5})	λ_3 (e Å^{-5})	ε
C$-$O	1.2565 (5)	0.461 (3)	0.796 (3)	2.722 (10)	−31.8 (3)	−25.08 (15)	−24.38 (16)	17.66 (12)	0.029 (9)
	1.258	0.430	0.827	2.545	−12.90	−24.40	−23.50	34.99	0.038
	1.258	0.410	0.848	2.594	−7.46	−25.37	−25.29	43.20	0.003
	1.258	0.421	0.837	2.578	−11.92	−24.62	−24.31	37.01	0.013
	1.258	0.427		2.536	−18.86	−23.33	−20.23	24.71	0.15
C$-$N	1.3384 (4)	0.542 (4)	0.796 (4)	2.359 (16)	−25.0 (3)	−20.29 (17)	−16.2 (2)	11.50 (16)	0.26 (2)
	1.341	0.471	0.870	2.326	−22.86	−21.77	−19.09	18.00	0.140
	1.341	0.449	0.892	2.376	−27.35	−21.51	−19.70	13.86	0.092
	1.341	0.466	0.874	2.339	−26.53	−20.19	−18.55	12.20	0.089
	1.343	0.440		2.538	−37.66	−27.34	−23.00	12.68	0.19
N$-$H1	1.005 (2)	0.751 8(12)	0.253 (2)	2.25 (2)	−30.9 (7)	−31.2 (3)	−28.6 (4)	28.94 (13)	0.091 (19)
	1.007	0.763	0.244	2.360	−48.78	−35.65	−33.92	20.79	0.051
	1.007	0.785	0.222	2.341	−47.27	−35.10	−33.50	21.33	0.048
	1.007	0.769	0.238	2.311	−48.54	−33.53	−31.90	16.89	0.051
	1.005	0.795		1.797	−30.44	−26.77	−25.54	21.88	0.05
N$-$H2	1.0020 (15)	0.7486 (18)	0.253 (2)	2.280 (13)	−34.6 (3)	−32.31 (19)	−30.10 (16)	27.78 (12)	0.073 (9)
	1.000	0.755	0.245	2.405	−49.67	−36.24	−34.45	21.01	0.052
	1.000	0.778	0.222	2.384	−48.20	−35.66	−34.02	21.48	0.048
	1.000	0.762	0.239	2.355	−49.45	−34.10	−32.43	17.07	0.052
	0.997	0.791		1.843	−33.37	−28.13	−26.93	21.68	0.05

3.3.1. Quantitative comparison of BCPs with periodic RHF and ZSTVF. Tables 5 and S5 compare the BCPs with the periodic RHF results and the data of ZSTVF. The C$-$O and C$-$N BCPs are always closer to C than to O and N atoms, and in the N$-$Hi bonds they are closer to the H than to the N atom. It is clear from the distances that both the periodic RHF calculations and ZSTVF show systematically more polarized bonds than the present density. Compared to our experimental density, $\rho(\mathbf{r}_c)$ of the C$-$O and C$-$N bonds is underestimated by the RHF calculations while those in N$-$H bonds are overestimated. In the ZSTVF study, the C$-$O and N$-$H bonds show smaller, and the C$-$N bond larger, electron densities than in the present.

The Laplacians also show large variations. Compared to the present results, the C$-$O Laplacian is consistently too small in the RHF calculations while the N$-$H values are too large. For the C$-$O bond, the erratic behaviour upon extension of the basis set indicates that the basis sets are inadequate. For all three basis sets, and especially for 6-31G(d,p), λ_3 is predicted to be far too large. For the N$-$H bonds, λ_1 and λ_2 are overestimated (too negative) while λ_3 is too small. As mentioned in the previous section, ZSTVF gives too small a Laplacian for the C$-$O bond. This is largely due to too large a value of λ_3.

In order to investigate the effect of basis set and electron correlation on CPs and integrated properties, we performed a large number of computations on urea (Birkedal & Schwarzenbach, 2004). These included non-correlated calculations (RHF), perturbation treatment of correlation (MP2, MP3, MP4SDQ), variational treatment of correlation (CISD) and a single density functional approach (B3LYP). Computations were done with different basis sets: 6-31G(nd,np) (n = 1, 2, 3), 6-311G(nd,np) (n = 1, 2, 3), 6-311++G, 6-311++G(3d,3p), cc-pVDZ and cc-pVTZ. These include some of the most frequently used double- and triple-zeta basis sets. We shall not

discuss these results in detail here but merely summarize some key results. For both the 6-31G(nd,np) and 6-311G(nd,np) series, it was found that the above-mentioned over-polarization of the C$-$O bond disappeared when more polarization functions were added [increasing n in (nd,np)]. This resulted in a larger absolute (more negative) value of the Laplacian at the bond critical point. The addition of diffuse functions did not influence this property. This shows that the oft-used basis sets 6-31G(d,p) and 6-311G(d,p), with or without diffuse functions, are not well adapted for the description of the strongly polarized C$-$O bond. The agreement with the present study was further improved by adding electron correlation.

These observations consistently indicate a deficiency in the computations, especially for the highly polarized C$-$O bond. The ZSTVF density shows many of the same problems as the calculations.

3.3.2. Integrated properties. Integrated atomic Laplacians, charges, volumes and dipole moments are given in Table 6, where they are compared with the corresponding values derived directly from the multipole model. This table also reports the properties obtained by integration of the theoretical data (Gatti, 1999). The superior precision of the present study is immediately seen by comparison of the monopole charges with those of ZSTVF, the monopole s.u.'s being lower by a factor of 2–3.5 in the present work. The ZSTVF monopole charges are equal to the present ones within three ZSTVF s.u.'s.

The integrated Laplacians, L, are all reasonably small indicating that the integrations over the atomic basins are sufficiently precise. This is reflected by the integrated volumes and charges that all deviate by less than 0.3% from the expected values ($V_{\text{molecule}} = 1/2V_{\text{cell}}$ and $q_{\text{molecule}} = 0$).

The integrated atomic charges obtained from the periodic RHF calculations are much larger than the experimental ones,

Table 6
Integrated properties for urea: Laplacian, charges and dipole moments.

L is the integrated Laplacian in units of 10^{-5} e Å^{-2}. Integrated volume V in Å^3 units, the three charges (q, q^{mono} and q^{mono}_{ZSTVF}) in e units. The right half of the table gives the atomic dipole moments and their contributions. All dipole contributions in units of e Å. The only non-zero d_x^a and d_y^a are $d_x^a(N) = 0.023$, $d_x^a(H1) = 0.055$ and $d_y^a(H1) = -0.002$ e Å. The first line gives the results of the present study, the three following lines present the periodic RHF results (Gatti, 1999) in the order 6-21G(d,p) (second line), 6-31G(d,p) (third line) and 6-311G(d,p) (fourth line). $\sum NH_2$, $\sum CO$, $\sum mol$ give sums over the NH$_2$ group, the CO group and the full molecule, respectively.

			Charges				Dipole moments AIM			Multipoles		
Ω	L	V	q	q^{mono}	q^{mono}_{ZSTVF}	Ω	d_z^a	d_z^{ct}	d_z	d_z^a	d_z^{ct}	d_z
C	19	4.35	1.667	−0.07 (4)	−0.03 (13)	C	0.113	2.564	2.677	−0.017 (9)	−0.11 (6)	−0.12 (6)
	−1176	3.33	2.322				0.049	3.571	3.620			
	−1192	3.07	2.478				0.048	3.812	3.860			
	−701	3.34	2.332				0.052	3.586	3.639			
O	20	17.58	−1.177	−0.41 (2)	−0.23 (7)	O	0.144	−3.290	−3.146	−0.071 (7)	−1.13 (6)	−1.21 (6)
	49	17.87	−1.429				0.221	−3.995	−3.773			
	31	18.51	−1.479				0.265	−4.136	−3.871			
	9	18.52	−1.431				0.210	−4.002	−3.791			
N	478	19.52	−1.214	−0.04 (5)	−0.30 (9)	N	−0.029	−1.018	−1.048	0.016 (8)	−0.03 (4)	−0.02 (4)
	83	19.78	−1.442				−0.069	−1.194	−1.263			
	447	20.19	-1.572				−0.078	−1.302	−1.380			
	190	19.72	−1.453				−0.073	−1.204	−1.276			
H1	−484	2.91	0.482	0.14 (2)	0.21 (4)	H1	−0.026	0.641	0.615	0.088 (9)	0.19 (3)	0.28 (3)
	−29	2.97	0.503				−0.032	0.670	0.638			
	37	2.65	0.541				−0.035	0.721	0.686			
	12	2.85	0.507				−0.034	0.675	0.641			
H2	−251	2.98	0.493			H2	0.064	−0.080	−0.016	−0.222 (13)	−0.022 (3)	−0.244 (14)
	−3	3.13	0.492				0.067	−0.080	−0.013			
	5	2.81	0.531				0.072	−0.087	−0.014			
	48	2.98	0.497				0.069	−0.081	−0.012			
$\sum NH_2$		25.40	−0.240	0.24 (6)	0.12 (11)	$\sum NH_2$	0.009	−0.458	−0.448	−0.119 (18)	0.13 (5)	0.01 (5)
		25.88	−0.448				−0.034	−0.604	−0.639			
		25.64	−0.500				−0.040	−0.667	−0.708			
		25.55	−0.450				−0.038	−0.610	−0.648			
$\sum CO$		21.93	0.490	−0.48 (5)	−0.26 (15)	$\sum CO$	0.257	−0.725	−0.469	−0.088 (11)	−1.24 (9)	−1.33 (9)
		21.20	0.893				0.270	−0.424	−0.153			
		21.59	0.999				0.312	−0.324	−0.012			
		21.85	0.900				0.263	−0.415	−0.153			
$\sum mol$		72.73	0.011	0.00 (9)	−0.02 (21)	$\sum mol$	0.275	−1.640	−1.365	−0.33 (3)	−0.98 (11)	−1.30 (11)
		72.95	−0.002				0.202	−1.632	−1.430			
		72.87	−0.000				0.232	−1.659	−1.427			
		72.96	−0.000				0.186	−1.635	−1.449			

especially for C atoms, where all three RHF calculations give charges larger than 2.3 e. The aforementioned investigation of basis set and correlation dependence of the BCPs was extended to integrated atomic properties (Birkedal & Schwarzenbach, 2004). The conclusion was clear: the very large atomic charge on the C atom is due to the neglect of electron correlation. The present experiment provides a target value against which new calculations can be validated.

The molecular dipole moment vector can be written as a sum over atomic contributions $\mathbf{d} = \sum_\Omega q(\Omega)\mathbf{X}_\Omega + \sum_\Omega \mathbf{M}(\Omega) = \mathbf{d}^{ct} + \mathbf{d}^a$, where $\mathbf{X}_\Omega$ is the nuclear position vector and $\mathbf{M}(\Omega)$ is the first moment of the atomic charge distribution: $\mathbf{M}(\Omega) = -e \int_\Omega \mathbf{r}_\Omega \rho(\mathbf{r})\,d\mathbf{r}$ (Bader, 1994). For the following, we define a Cartesian coordinate system with the z axis along the C—O bond and the y axis perpendicular to the molecule. Owing to the molecular site symmetry, only d_z is non-zero. The molecular dipole moment from the AIM integrated properties and the multipole model are equal within one s.u. even though the individual atomic contributions are completely different. The values 1.37 and 1.30 (11) e Å correspond to 6.56 and 6.2 (5) D,

respectively. For the multipole dipole, the charge contribution is generally small except for the O atom, which dominates the total dipole moment. The net contribution of the NH$_2$ group is almost zero. This is in contrast to the AIM partitioning where the NH$_2$ groups contribute 66% of the total moment. These differences are due to the completely different atomic charges.

The AIM molecular dipole moments from the periodic RHF calculations are 6.87, 6.85 and 6.96 D for 6-21G(d,p), 6-31G(d,p) and 6-311G(d,p), respectively. The influence of geometry and/or computational precision can be appreciated by comparison of the 6-31G(d,p) moments at the 123 and 12 K SCM geometries: for the 12 K geometry, Gatti *et al.* (1994) found 7.03 D. This variation reflects the level of precision that can be expected from these calculations. In this view, the agreement between the periodic RHF calculations and the present experiment is good.

From X-ray diffuse scattering along the *c* axis of urea, Lefebvre (1973) derived acoustic and optical phonon dispersion curves. By using a lattice dynamical model, the dipole moment was estimated to be 4.66 D. Later, based on coherent

inelastic neutron scattering on deuterated urea, Lefebvre *et al.* (1975) established an improved force-constant model that yielded a dipole moment of 3.99 D. Estimates of the solution and gas-phase dipole moment are collected in Table S9. They range from 3.83 to 6.38 D with a mean value of 5.1 D. Even for measurements in the same solvent, variations are large. In water at room temperature, the values range from 4.20 to 5.79 D with an average of 5.0 D. In view of the expected dipole enhancement in the solid, the Lefebvre (1973) and Lefebvre *et al.* (1975) values appear to be somewhat small. In Gatti *et al.*'s (1994) RHF/6-31G(d,p) calculations, a clear enhancement was seen: the molecular dipole moment in the bulk was found to be larger by 1.9 D than the isolated molecule moment with the same geometry. A similar, but somewhat smaller, enhancement of 1.41 D was found by multipole modelling of RHF/DZPT structure factors by Spackman *et al.* (1999). If this enhancement can be taken as valid, a value of about 6.5–7 D would be expected in the solid state in perfect agreement with the present values. Spackman *et al.* (1988) analysed the SCSS multipole model and found a dipole moment of 5.4 (5) D – not inconsistent with the present results. ZSTVF obtained the rather small value of 3.8 D.

3.4. Multipole refinement of a non-centrosymmetric system

The structure of urea is non-centrosymmetric and, with the exception of symmetry-restricted phases, the structure-factor phases can take any value between 0 and 2π. Therefore, it can be expected that modelling the charge density will be more difficult than for centrosymmetric structures. In a series of detailed studies on noise-free *ab initio* data sets, Spackman and co-workers have shown that the multipole model is capable of recovering phases (Spackman & Byrom, 1997) and interaction densities (Spackman *et al.*, 1999)[6] faithfully – at least in well behaved systems like urea. de Vries *et al.* (2000) investigated the influence of noise on the modelling of the interaction density with structure factors calculated with periodic denssity functional theory (DFT) at the B-PWGGA/6-21G(d,p) level. They calculated 412 structure factors matching the data set of ZSTVF and included temperature effects by applying the SCM 123 K ADPs on Hirshfeld partitioned atomic densities. This data set was then used as input for multipole modelling. The multipole model was rather restricted: the core populations of C, O and N atoms were kept fixed at 2, one κ parameter only was used for the valence shells of the three heavy atoms and the radial functions of the H atoms were kept fixed. The refinement included the hexadecapole level on C, N and O atoms and quadrupoles on H atoms. This model recuperated the salient features of the interaction density. They then proceeded by including noise in the data by adding a random fraction of the ZSTVF s.u.'s to each structure factor. The ensuing refinement did not recover the interaction density. Therefore the authors concluded that a data set like ZSTVF is not of sufficient quality for modelling

---

[6] The interaction density is the difference between a theoretical molecular density and the experimental one.

the interaction density and thus the intermolecular interactions. They conclude by adding the caveat '. . . an experiment in which more structure factors are measured more accurately would give better results'. It would appear that the present experiment has achieved exactly this.

4. Conclusions

The present data set of urea is of unprecedented resolution and precision. The refined nuclear parameters are in good agreement with the SCM neutron results and additionally show that non-negligible anharmonic contributions to the thermal motion are present at N and C atoms. The features of the derived static charge density fit very well into the general picture provided by high-precision studies of other systems. It can thus safely be stated that the most precise electron density of urea available to date has been extracted from the present data set. This result could not have been achieved without the use of synchrotron radiation and very high precision instrumentation.

Our results underline the need for improving the level of theoretical calculations. The 6-31G and 6-311G series of basis sets were found to be inadequate unless extensive sets of polarization functions are added. These basis sets have a common drawback: the valence *s* and *p* functions have a common exponent. This was originally motivated by limited computer power. For relatively small systems (including also molecules larger than urea), this limitation is no longer justified and other basis sets should be used. For comparison of integrated properties, calculations must include correlation effects. Note that these deficiencies of current *ab initio* calculations are particularly prominent in urea because of the highly polarized C—O bond. In less extreme systems, the effects are smaller and more moderate levels of theory can be expected to function well.

In view of the current active discussions on the choice of radial basis functions, it would appear that studies like the present one, where the focus is on extreme precision for a small systems amenable to calculation, are of the utmost importance. In addition, it would be advantageous if also the *average* charge-density study would extend to higher angles and higher precision thereby allowing more extensive modelling. Finally, we recommend a more flexible attitude of the charge-density community regarding the choice and refinement of radial basis functions.

References

Andersson, O., Matsuo, T., Suga, H. & Ferloni, P. (1993). *Int. J. Thermophys.* **14**, 149–158.

Andersson, O. & Ross, R. G. (1994). *Int. J. Thermophys.* **15**, 513–524.

Anzenbacher, P. Jr, Jursíková, K., Lynch, V. M., Gale, P. A. & Sessler, J. L. (1999). *J. Am. Chem. Soc.* **121**, 11020–11021.

Bader, R. F. W. (1994). *Atoms in Molecules. A Quantum Theory*, first paperback edition (with corrections). Oxford: Clarendon Press.

Birkedal, H. (2000). PhD thesis, University of Lausanne, Switzerland.

Birkedal, H. & Schwarzenbach, D. (2004). In preparation.

Becker, P. J. & Coppens, P. (1974). *Acta Cryst.* A**30**, 129–147.

Blessing, R. H. (1987). *Crystallogr. Rev.* **1**, 3–58.

Bonin, M., Marshall, W. G., Weber, H.-P. & Toledano, P. (1999). ISIS99. The ISIS Facility Annual Report 1998–1999. ISIS Neutron Facility, Rutherford Appleton Laboratory, Chilton, Didcot, Oxon, England.

Bonomo, L., Solari, E., Toraman, G., Scopelliti, R., Latronico, M. & Floriani, C. (1999) *J. Chem. Soc. Chem. Commun.* pp. 2413–2414.

Bürgi, H.-B. & Capelli, S. (2000). *Acta Cryst.* A**56**, 403–412.

Bürgi, H.-B., Capelli, S. & Birkedal, H. (2000). *Acta Cryst.* A**56**, 425–435.

Bürgi, H.-B. & Förtsch, M. (1999). *J. Mol. Struct.* **485–486**, 457–463.

Capelli, S., Förtsch, M. & Bürgi, H.-B. (2000). *Acta Cryst.* A**56**, 413–424.

Clementi, E. & Roetti, C. (1974). *At. Data Nucl. Data Tables*, **14**, 177–478.

Dittrich, B., Flaig, R., Koritsánszky, T., Krane, H.-G., Morgenroth, W. & Luger, P. (2000). *Chem. Eur. J.* **6**, 2582–2589.

Dixon, D. A. & Matsuzawa, N. (1994). *J. Phys. Chem.* **98**, 3967–3977.

Dovesi, R., Causa, M., Orlando, R., Roetti, C. & Saunders, V. R. (1990). *J. Chem. Phys.* **92**, 7402–7411.

Dunitz, J. D., Harris, K. D. M., Johnston, R. L., Kariuki, B. M., MacLean, E. J., Psallidas, K., Schweizer, W. B. & Tykwinski, R. R. (1998). *J. Am. Chem. Soc.* **120**, 13274–13275.

Figgis, B. N., Iversen, B. B., Larsen, F. K. & Reynolds, P. A. (1993). *Acta Cryst.* B**49**, 794–806.

Finger, L. W., Cox, D. E. & Jephcoat, A. P. (1994). *J. Appl. Cryst.* **27**, 892–900.

Flaig, R., Koritsanszky, T., Janczak, J., Krane, H.-G., Morgenroth, W. & Luger, P. (1999). *Angew. Chem. Int. Ed. Engl.* **38**, 1397–1400.

Flaig, R., Koritsanszky, T., Zobel, D. & Luger, P. (1998). *J. Am. Chem. Soc.* **120**, 2227–2238.

Flensburg, C., Larsen, S. & Stewart, R. F. (1995). *J. Phys. Chem.* **99**, 10130–10141.

Flensburg, C. & Madsen, D. (2000). *Acta Cryst.* A**56**, 24–28.

Gatti, C. (1999). Personal communication.

Gatti, C. & Cargnoni, F. (1997). III Convegno Nazionale di Informatica Chim, Napoli, Italy, 27 February–1 March 1997, extended abstracts, pp. 125–128.

Gatti, C., Saunders, V. R. & Roetti, C. (1994). *J. Chem. Phys.* **101**, 10686–10696.

Godfrey, P. D., Brown, R. D. & Hunter, A. N. (1997). *J. Mol. Struct.* **413–414**, 405–414.

Ha, T.-K. & Puebla, C. (1994). *Chem. Phys.* **181**, 47–55.

Hamilton, W. C. (1965). *Acta Cryst.* **18**, 502–510.

Hehre, W. J., Ditchfield, R., Stewart, R. F. & Pople, J. A. (1970). *J. Chem. Phys.* **52**, 2769–2773.

Hehre, W. J., Stewart, R. F. & Pople, J. A. (1969). *J. Chem. Phys.* **51**, 2657–2664.

Keuleers, R., Desseyn, H. O., Rousseau, B. & Van Alsenoy, C. (1999). *J. Phys. Chem. A*, **103**, 4621–4630.

Larson, A. C. & Von Dreele, R. B. (1994). GSAS, Los Alamos National Laboratory Report LAUR 86–748. Los Alamos, NM 87545, USA.

LeBail, A., Duroy, H. & Fourquet, J. L. (1988). *Mater. Res. Bull.* **23**, 447–452.

Lefebvre, J. (1973). *Solid State Commun.* **13**, 1873–1875.

Lefebvre, J., More, M., Fouret, R., Hennion, B. & Currat, R. (1975). *J. Phys. C Solid State Phys.* **8**, 2011–2021.

MacLean, E. J., Harris, K. D. M., Kariuki, B. M., Kitchin, S. J., Tykwinski, R. R., Swainson, I. P. & Dunitz, J. D. (2003). *J. Am. Chem. Soc.* **125**, 14449–14451.

Madsen, D., Flensburg, C. & Larsen, S. (1998*a*). *J. Phys. Chem. A*, **102**, 2177–2188.

Madsen, G. K. H., Iversen, B. B., Larsen, F. K., Kapon, M., Reisner, G. M. & Herbstein, F. H. (1998*b*). *J. Am. Chem. Soc.* **120**, 10040–10045.

Mathiesen, R. H. (2001). *J. Appl. Cryst.* **34**, 785.

Miao, M. S., Van Doren, V. E., Keuleers, R., Desseyn, J. A., Van Alsenoy, C. & Martins, J. L. (2000). *Chem. Phys. Lett.* **316**, 297–302.

Pisani, C. (1996). Editor. *Quantum-Mechanical Ab Initio Calculation of the Properties of Crystalline Materials. Lecture Notes in Chemistry*, No. 67. Berlin: Springer-Verlag.

Pisani, C., Dovesi, R. & Roetti, C. (1988). Editors. *Hartree–Fock Ab Initio Treatment of Crystalline Systems. Lecture Notes in Chemistry*, No. 48. Berlin: Springer-Verlag.

Rasul, G., Prakash, G. K. S. & Olah, G. A. (1994). *J. Org. Chem.* **59**, 2552–2556.

Rousseau, B., Van Alsenoy, C., Keuleers, R. & Desseyn, H. O. (1998). *J. Phys. Chem. A*, **102**, 6540–6548.

Roversi, P., Barzaghi, M., Merati, F. & Destro, R. (1996). *Can. J. Chem.* **74**, 1145–1156.

Ruehrwein, R. A. & Huffman, H. M. (1946). *J. Am. Chem. Soc.* **68**, 1759–1761.

Spackman, M. A. & Byrom, P. G. (1997). *Acta Cryst.* B**53**, 553–564.

Spackman, M. A., Byrom, P. G., Alfredsson, M. & Hermansson, K. (1999). *Acta Cryst.* A**55**, 30–47.

Spackman, M. A., Weber, H. P. & Craven, B. M. (1988). *J. Am. Chem. Soc.* **110**, 775–782.

Stephens, P. W. (1999). *J. Appl. Cryst.* **32**, 281–289.

Stewart, R. F. (1976). *Acta Cryst.* A**32**, 565–574.

Stewart, R. F. (1977). *Isr. J. Chem.* **16**, 124–131.

Stewart, R. F., Spackman, M. A. & Flensburg, C. (1998). *VALRAY98 Users Manual.* Carnegie-Mellon University, USA, and University of Copenhagen, Denmark.

Swaminathan, S., Craven, B. M. & McMullan, R. K. (1984). *Acta Cryst.* B**40**, 300–306.

Swaminathan, S., Craven, B. M., Spackman, M. A. & Stewart, R. F. (1984). *Acta Cryst.* B**40**, 398–404.

Thompson, P., Cox, D. E. & Hastings, J. B. (1987). *J. Appl. Cryst.* **20**, 79–83.

Thorkildsen, G., Larsen, H. B., Mathiesen, R. H. & Mo, F. (2000). *J. Appl. Cryst.* **33**, 49–51.

Thorkildsen, G., Mathiesen, R. H. & Larsen, H. B. (1999). *J. Appl. Cryst.* **32**, 943–950.

Volkov, A., Abramov, Y., Coppens, P. & Gatti, C. (2000). *Acta Cryst.* A**56**, 332–339.

Vries, R. Y. de, Feil, D. & Tsirelson, V. G. (2000). *Acta Cryst.* B**56**, 118–123.

Wal, R. J. van der & Stewart, R. F. (1984). *Acta Cryst.* A**40**, 587–593.

Wang, K. & Reeber, R. R. (2000). *Appl. Phys. Lett.* **76**, 2203–2204.

Zachariasen, W. H. (1967). *Acta Cryst.* **23**, 558–564.

Zavodnik, V., Stash, A., Tsirelson, V., de Vries, R. & Feil, D. (1999). *Acta Cryst.* B**55**, 45–54.